NJC

PAPER

View Article Online
View Journal | View Issue

Cite this: *New J. Chem.*, 2016, **40**, 7846

Characterization of a highly efficient N-doped TiO_2 photocatalyst prepared *via* factorial design†

Karen A. Borges,[a] Lidiaine M. Santos,[a] Roberto M. Paniago,[b] Newton M. Barbosa Neto,[c] Jenny Schneider,[d] Detlef W. Bahnemann,[de] Antonio Otavio T. Patrocinio*[a] and Antonio Eduardo H. Machado*[a]

Received (in Nottingham, UK) 4th March 2016,
Accepted 19th July 2016

DOI: 10.1039/c6nj00704j

www.rsc.org/njc

The preparation of titanium dioxide nanoparticles doped with nitrogen for application as a photocatalyst in the decomposition of azo dyes was optimized by factorial planning. Five variables were evaluated and the results showed that the stirring method of the reaction medium, the nitrogen source and the calcination temperature are the determining parameters that affect the photocatalytic activity. With this methodology, it was possible to obtain an optimized photocatalyst (K1) with high surface area and high mineralization efficiency (100%) of the dye Ponceau 4R under solar irradiation. K1, its non-doped version and the worst photocatalyst obtained by the factorial planning (K2) were characterized by several techniques to rationalize the different behaviors. The observed mineralization rate constants under artificial UV-A radiation were in the order of 10^{-2}, 10^{-4} and 10^{-3} min^{-1}, respectively, for K1, K2 and the non-doped oxide. As shown by N_2 sorption isotherms, the powders exhibited large variations in porosity as well as in the specific surface area, with values ranging from 63.03 m^2 g^{-1} for K1 to 12.82 m^2 g^{-1} for K2. Infrared spectra showed that the calcination of the doped oxides between 300 and 500 °C leads to considerable loss of the nitrogen content, which is corroborated by XPS measurements that also indicate the presence of oxygen vacancies on their surfaces. Nanosecond transient absorption measurements show that the electron–hole half-lifetime in K1 is 870 ns, *ca.* two times longer than that observed for the other photocatalysts. Additionally, dye degradation studies under solar radiation reveal that K1 is *ca.* 28% faster than the non-doped TiO_2 under similar conditions. This higher photoactivity for K1 is attributed to its extended visible light absorption and the optimized morphological and electronic properties.

1. Introduction

Nanostructured titanium dioxide (TiO_2) has attracted interest in several research areas, including photoelectrochemical applications.[1–4] The photocatalytic efficiency of TiO_2 depends on its structural and morphological characteristics, which are related to the method of synthesis used in its preparation.[5–8] Typically, the crystalline structure needs to be controlled (anatase is ascribed as the most active one) along with high specific surface area and adequate pore size to allow the diffusion and adsorption of the reacting species.[9,10]

One of the main limitations of TiO_2 is its band gap energy (3.2 eV), which limits its use under solar radiation.[11,12] However, doping and other alternatives[13–17] can introduce new intra-band gap electronic states in TiO_2, enabling light harvesting in the visible region.[18–21] Among the different dopants typically employed, the use of nitrogen arises as a viable possibility.[22–24] Being less electronegative than oxygen (3.0 and 3.5 eV respectively), the incorporation of nitrogen introduces electronic states above the valence band of TiO_2, causing the reduction of its band gap excitation energy.[25] Nitrogen doped oxides can be produced by thermal treatment under ammonia flow or by wet methodologies using different sources such as NH_4OH, NH_4Cl, thiourea or urea.[26–31]

Although there is a considerable number of studies involving the doping of TiO_2 by nitrogen[32–35] systematic studies on the

[a] *Laboratory of Photochemistry and Materials Science, Institute of Chemistry, Universidade Federal de Uberlandia, Uberlandia, 38400-902, Minas Gerais, Brazil. E-mail: otaviopatrocinio@ufu.br, aehmachado@gmail.com*
[b] *Universidade Federal de Minas Gerais, Belo Horizonte, 31270-901, Minas Gerais, Brazil*
[c] *Instituto de Ciências Exatas e Naturais, Universidade Federal do Pará, Belém, 66075-110, Pará, Brazil*
[d] *Institut für Technische Chemie, Leibniz Universität Hannover, Callinstrasse 3, D-30167, Hannover, Germany*
[e] *Laboratory for Nanocomposite Materials, Department of Photonics, Faculty of Physics, Saint-Petersburg State University, Ulianovskaia str. 3, Peterhof, Saint-Petersburg, 198504, Russia*

† Electronic supplementary information: Fit parameters for Rietveld analyses of the XRD data; DOC decay as a function of irradiation time for the photocatalysts studied; experimental data for construction of the response surface of the mineralization efficiency as a function of sintering temperature and time; N_2 sorption curves for the K1, K2 and bare TiO_2; Rietveld analyses of the XRD data; and FTIR spectra of K1 before and after sintering. See DOI: 10.1039/c6nj00704j

relation between the variables involved in the synthesis and the photocatalytic activity were found only in a reduced number.[36–38] As the different parameters may interact between themselves, multivariate data analysis appears as a powerful tool to obtain highly efficient photocatalysts. Chemometrics methods have been largely applied in chemical analysis, spectroscopy and process optimization.[39–41] In photocatalysis, they have been used mainly on the investigation of the synergic interactions of key physicochemical parameters that affect the photocatalytic efficiency (pH, reaction times, relative concentrations *etc.*).[42–47] Only in a few works in the literature, chemometrics tools have been used to evaluate the synthetic parameters employed in the photocatalyst preparation.[48]

In the present study, we have used experimental factorial design (screening and response surface experiments) to identify the most important synthetic variables that affect the photocatalytic activity of N-doped TiO_2 catalysts. The photocatalytic activity of the synthesized materials was quantified using the Ponceau 4R (P4R) dye as the target compound. Different characterization techniques were employed to establish direct relationships between the structure and photocatalytic efficiency.

2. Materials and methods

2.1. Synthesis

TiO_2 powders were prepared by the precipitation method.[49,50] Briefly, 5 mL (17 mmols) of the metal precursor, titanium(IV) isopropoxide (Aldrich, 97%), was dissolved in 13 mL of 2-propanol (HPLC grade, VETEC). The resulting solution was kept under stirring, while 50 mL of deionized water was slowly dropped to yield a white precipitate using a jacketed addition funnel. The water temperature was controlled using a cooling thermostat bath connected to the funnel. Two different stirring methods were employed by using a magnetic stirrer or an ultrasound bath (70 W, 40 Hz). The precipitate was washed with deionized water, centrifuged at room temperature, and dried at 70 °C.

Nitrogen doping was carried out by suspending the powder into 30% m/m urea (pH = 7) or 30% m/m NH_4OH solution (pH = 8). The system was kept under stirring for 24 h and then let to rest in the dark for two days. After that, the precipitate was washed with deionized water, centrifuged at room temperature, and dried at 70 °C. The samples were submitted to a thermal treatment at two different temperatures (400 °C and 500 °C) for 3 hours.

The influence of the synthesis conditions and thermal treatment on the photocatalytic activity of TiO_2 powders was analyzed through a multifunctional experimental design. The defined variables, as well as their low and high values are summarized in Table 1. Such values were selected based on our previous studies and also on different works in the literature, in which one or more parameters were studied individually. The software package Statistica 7.0 (StatSoft, Inc. Tulsa, USA) was used to generate the experimental matrix, obeying a 2^{5-1} fractional factorial design. The response of interest was defined as the Ponceau 4R mineralization rate. After evaluation of the multivariate analysis results, a central composite design (CCD)[36] was applied to analyze the relationship between the sintering temperature and time on the N-doped TiO_2 photocatalytic activity.

Table 1 Experimental variables and their low and high values employed in the 2^{5-1} fractional factorial design

	Level	
Variable	Low (−1)	High (+1)
(1) Water temperature	3 °C	25 °C
(2) Stirring method	Ultrasound	Magnetic
(3) Nitrogen source	NH_4OH	Urea (CH_4N_2O)
(4) Peptizing time	1 hour	2 hours
(5) Sintering temperature	400 °C	500 °C

2.2. Methods

The samples were characterized by X-ray diffraction, using a Shimadzu XRD-6000 diffractometer, with a CuKα (λ = 1.54148 nm) monochromatic source. Crystalline silicon was used as the diffraction standard. The diffractograms were collected between 19° and 90° at 0.5° min^{-1}. Rietveld analyses of the XRD data were done using the FullProf software. Fit parameters can be found in the ESI† (Table S1). As fitting criteria, the ratio between the weight factor (R_{wp}) and the expected factor (R_{exp}) was employed, which should be closer to 1 ($R_{wp} = R_{exp}$).

The specific surface area, volume and pore diameter were measured towards N_2 adsorption/desorption isotherms using the BET methodology[51] and a Micrometrics ASAP 2020 surface analyzer. Scanning transmission electron microscopy (STEM) was carried out using a FEI Inspect F50 microscope located at the Brazilian Nanotechnology National Laboratory (LNNano) and operated at 30 kV.

Diffuse reflectance spectra of the synthesized oxides were acquired at room temperature using a double beam Shimadzu UV-1650 spectrophotometer equipped with an integration sphere. Barium sulfate was used as blank. The band gap energy was estimated by the Kubelka–Munk function.[52] FTIR spectra were acquired in the range between 500 and 4000 cm^{-1} on a SHIMADZU IR Prestige-21 spectrometer, using potassium bromide pellets with the synthesized oxides. XPS spectra were obtained as previously described[53,54] using a VG Scientific ESCALAB 220 iXL surface analysis system equipped with an Mg/Al double anode monochromator and an electron spherical analyzer. C1s peak at 284.6 eV was employed as the internal reference.

Transient absorption spectroscopy (TAS) was carried out employing a LKS80 nanosecond laser flash photolysis spectrometer (Applied Photophysics) equipped with the proper diffuse reflectance accessory as described previously.[55] The samples were excited in a quartz cuvette using a LPX 200 excimer laser from Lambda Physics (XeF; λ_{exc} = 351 nm; 14 mJ per pulse, illumination area of laser beam: 0.5 cm^2). The transient signals were collected using a PMT connected to a computer interfaced to a DSO9064A oscilloscope (Agilent). The transient decay was then recorded using the oscilloscope as the voltage changes,

and the data points were recalculated to the final signal ΔJ according to eqn (1), in which I_0 is the incident intensity of the analyzing light; J_0 is the diffuse reflected light without the laser pulse (ground light level); and J_x is the diffuse reflected light with the laser pulse. It has been reported that for TiO_2 the ΔJ value can be correlated with the transient absorption if ΔJ is less than 0.3,[56,57] thus to describe the results obtained by detection of the diffuse reflected light, the term transient absorption will be referred to.

$$\Delta J = \frac{J_0/I_0 - J_x/I_0}{J_0/I_0} = \frac{J_0 - J_x}{J_0} \quad (1)$$

Raman spectra were acquired at room temperature using a triple-grating Jobin Yvon T64000 spectrometer, collecting the scattered light with backscattering configuration. Samples were excited at 514 nm, delivered by an argon laser and the spectrometer slits were set for a resolution of 0.6 cm^{-1}.

2.3. Lab-scale photodegradation tests

The photocatalytic activity of the as prepared N-doped TiO_2 was evaluated through degradation of the azo-dye Ponceau 4R (P4R) using UV-A radiation. A detailed description of the experimental setup can be found elsewhere.[58] Briefly, 100 mg L^{-1} of photocatalyst were suspended in 4 L of a 30 mg L^{-1} (6.44×10^{-5} mol L^{-1}) aqueous solution of P4R in an annular borosilicate reactor connected to a water cooled reservoir through a peristaltic pump. The suspension was kept in the dark and under stirring for 10 minutes to reach the adsorption equilibrium. After that, a 400 W high pressure mercury vapor lamp centered at the reactor was turned on. The photonic flux of the lamp was 3×10^6 Einsteins s^{-1}. Aliquots were taken every 20 minutes up to 140 minutes of reaction and filtered using 0.45 μm membranes prior to the analyses. A Shimadzu TOC-VCPH analyzer was used to estimate the amount of dissolved organic carbon (DOC) during the experiments. P4R discoloration was probed spectrophotometrically at 507 nm, using a Shimadzu UV-1650PC spectrophotometer. Control experiments were performed in the absence of a catalyst to evidence the role of TiO_2 in the photochemical reaction.

2.4. Photocatalytic degradation under solar irradiation

For the assays using solar irradiation, aliquots of 50 mL of a mixture containing 15 mg L^{-1} of the P4R dye and 100 mg L^{-1} of the catalyst were exposed to solar irradiation in closed borosilicate glass vessels with an active area of 57 cm^2. A vessel was protected from light to be taken as a reference, with the others being irradiated. When the accumulated dose of UV-A was equal to 200 kJ m^{-2}, one vessel was taken for analysis and the others remained under irradiation. The UV-A radiation was monitored using a radiometer equipped with a PMA 2100 UV-A detector. The second vessel was taken after a 400 kJ m^{-2} UV-A dose and, finally, the last one at 600 kJ m^{-2}. The discoloration and the mineralization rates were probed, respectively, by spectrophotometry and DOC analyses. During the irradiation time, the temperature of the vessels varied from 25 to 35 °C. All photocatalysts were tested simultaneously, allowing direct comparisons on their respective photoactivities.

3. Results and discussion

3.1. Experimental factorial design applied to the preparation of N-TiO_2

The mineralization of P4R solutions, expressed as percentages of dissolved organic carbon $\left(100 \times \frac{DOC}{DOC_0}\right)$, after 140 minutes under artificial UV-A irradiation in the presence of different N-doped TiO_2 photocatalysts and the corresponding preparation conditions selected in the multivariate design are presented in Table 2. In the ESI,† it can be found that the DOC decays as a function of irradiation time for the catalysts studied, as well as for the direct photolysis of dye solution in the absence of a photocatalyst. The percentages of mineralization mediated by the photocatalysts synthesized in this work are systematically higher than that obtained by direct photolysis, when only

Table 2 Parameters used in the multivariate experimental design related for each synthesized N-doped TiO_2 photocatalyst and the achieved percentages of P4R mineralization (DOC removal). The values +1 (high) and −1 (low) are related, respectively, to the high and low levels of the studied variables

Catalyst	Water temperature	Stirring method	Doping source	Peptization time	Sintering temperature	Mineralization (±2%)
1	−1	−1	−1	−1	+1	28.93
2	+1	−1	−1	−1	−1	33.13
3	−1	+1	−1	−1	−1	53.00
4	+1	+1	−1	−1	+1	45.00
5	−1	−1	+1	−1	−1	29.13
6	+1	−1	+1	−1	+1	19.30
7	−1	+1	+1	−1	+1	24.15
8	+1	+1	+1	−1	−1	41.77
9	−1	−1	−1	+1	−1	41.83
10	+1	−1	−1	+1	+1	19.30
11	−1	+1	−1	+1	+1	40.73
12	+1	+1	−1	+1	−1	56.23
13	−1	−1	+1	+1	+1	15.13
14	+1	−1	+1	+1	−1	18.23
15	−1	+1	+1	+1	−1	43.33
16	+1	+1	+1	+1	+1	27.73

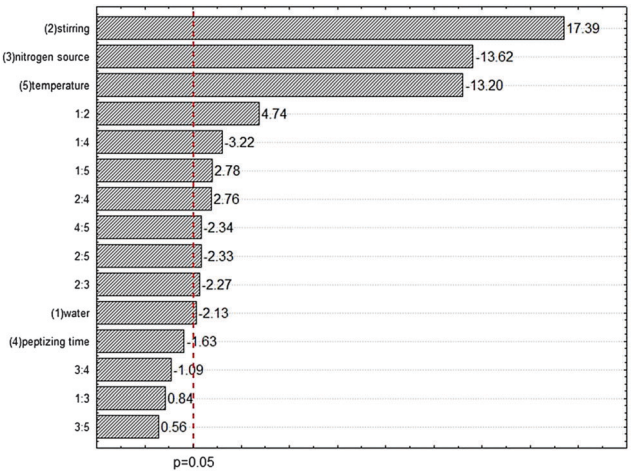

Fig. 1 Pareto's chart obtained from 2^{5-1} fractional factorial design.

12.70% of mineralization was achieved after 140 minutes of irradiation.

From the Pareto's chart, obtained by the analysis of the multivariate data, Fig. 1, it is possible to evaluate the influence of each variable and determine the best conditions of synthesis for obtaining an optimized N-doped TiO_2 photocatalyst.

The analysis reveals that the stirring method (2), nitrogen source (3) and sintering temperature (5) exert significant influence on the photocatalytic efficiency of the N-doped TiO_2 samples. The stirring method (2) has a positive correlation with the dye mineralization, which means that the photocatalytic process is favored when this variable is selected to be of high level. On the other hand, the variables (3) and (5) have a negative effect on mineralization. Therefore, the photocatalytic activity is favored if they are selected to be of low level. The variables water temperature (1) and peptizing time (4) by themselves have little influence on mineralization.

The multivariate analysis allows estimating the influence of the interaction between two variables on the efficiency of the photocatalytic process. It can be observed that the interactions between the variables 1 and 2 (1 : 2) and 1 and 5 (1 : 5) are significant and positive. It means that such variables when kept at a high level favor dye degradation. The interaction between variables 1 and 4 (1 : 4) is significant, but the result is negative for mineralization. The inversion of the level for one of these variables tends to cause a positive response. Variable 4 (peptizing time) was chosen to be inverted since it is less significant by itself. Then, it was set to the high level. Therefore, the best conditions for the preparation of N-doped TiO_2 powders with high photocatalytic activity are summarized in Table 3.

Photodegradation tests employing a catalyst prepared under the conditions shown in Table 3 resulted in (53 ± 2)% mineralization of the organic dye. This result is experimentally similar to that observed for the catalysts #12 and 3 (Table 2). So far, these results corroborate the conclusion taken from the multivariate analysis, since the difference in the preparation between the best catalyst defined by the statistical methodology and the catalysts #3 and #12 is related to the variables 1 and 4, which have a small influence on the photoresponse. The statistical method indicates what is physically expected: with lower water temperatures, a longer peptizing time is required and should yield more homogeneous and smaller particles, leading to improvements in the photocatalytic activity.

Table 3 Better experimental conditions found to prepare N-doped TiO_2, defined by experimental design

Variable	Conditions
(1) Water temperature	3 °C
(2) Stirring method	Magnetic
(3) Nitrogen source	NH_4OH
(4) Peptizing time	2 hours
(5) Sintering temperature	(Favored at the low level, 400 °C)

Additionally to the multivariate analysis, the central composite design (CCD) method was employed to identify the best conditions (temperature and time) for the thermal treatment of N-doped TiO_2 catalysts. For this, the other variables (1 to 4) have been maintained as shown in Table 3. The estimated ranges for temperature and time were, respectively, 300–450 °C and 3–5 hours, based on the results of the 2^{5-1} fractional factorial design. The fit of the mineralization efficiency as a function of sintering temperature and time resulting in the response surface is shown in Fig. 2 (experimental data can be seen in Table S2, ESI†).

The CCD data allowed determining the optimum sintering temperature and time regarding P4R degradation by N-doped TiO_2, which are, respectively, 333 °C and 4.2 hours. Nevertheless, it can be concluded from the surface response that catalysts treated at 330–400 °C for 4–5 hours should exhibit higher photocatalytic activities.

3.2. Morphological and electronic characterization of the as-prepared N-TiO_2 photocatalysts

Different characterization techniques were employed on the as-prepared catalysts in order to correlate their photocatalytic

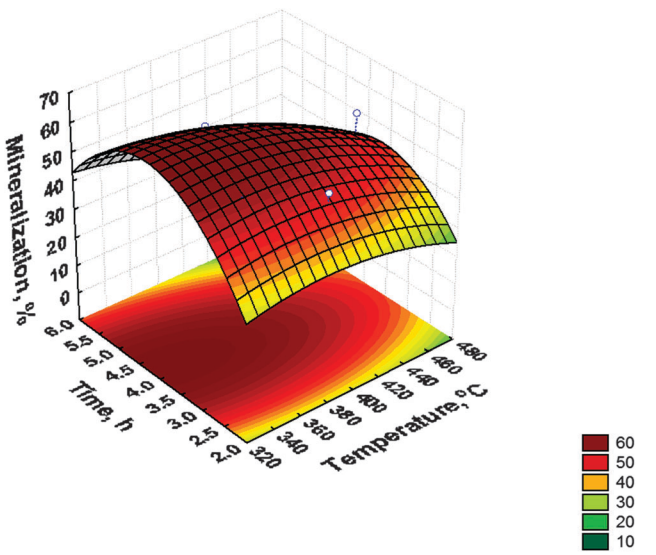

Fig. 2 Surface response showing the correlation between mineralization efficiencies, sintering temperature and time.

activity and preparation conditions with the morphological, structural and electronic properties. As a matter of comparison, the catalysts named as K1 and K2 were selected from the multivariate analysis, since the former exhibits the best mineralization of P4R (64%), while K2 furnished poor photocatalytic activity (~8%). In Table 4, the preparation conditions of K1 and K2 are presented, along with their respective photocatalytic performances. To clearly show the role of nitrogen as a modifier, a TiO_2 sample was obtained under the same conditions of K1, but without the addition of NH_4OH to the reaction medium. The apparent rate constants were determined following the Langmuir–Hinshelwood kinetics model.[59]

Firstly, N_2 adsorption/desorption isotherms were obtained in order to determine the specific surface area and other surface parameters, accordingly to the B. J. H. methodology,[51] Table 4. The isotherms of K1, K2 and also that for the bare oxide can be classified as type IV according to IUPAC,[60] which is typical for mesoporous materials (the N_2 sorption isotherms as well as the pore size distribution curves can be found in Fig. S3 of the ESI†). The specific surface area of K1 is about five times higher than the one of K2, while its pore volume is 75% larger. The results indicate that, in K1, there are more available adsorption sites outside the pore walls, which can be related to the presence of less aggregated particles. Looking at the preparation conditions, Table 4, the higher surface area of K1 should be a consequence of the smaller sintering temperature, which avoids the particle necking. This behavior can be seen in the STEM images of K1 and K2, Fig. 3. Additionally, the different shapes of the hysteresis in N_2 adsorption/desorption isotherms obtained for K1 and K2 indicate distinct surface textures (pore size, geometry, connectivity *etc.*). The better morphological parameters of K1 favor the adsorption of P4R and water molecules and should yield a higher density of active sites.[61]

It is noteworthy to observe that the surface area of a TiO_2 powder prepared under the same conditions of K1 but without the addition of NH_4OH exhibits higher surface area. This is likely due to the catalytic effect of OH^- ions on the hydrolysis of the Ti^{4+} precursor that leads to a higher particle growth. Nevertheless, as shown in Table 4, the higher surface area of bare TiO_2 does not lead to a higher P4R mineralization.

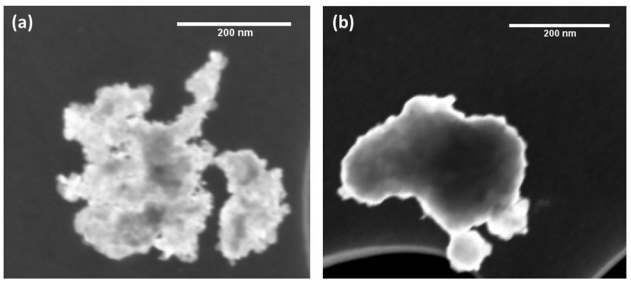

Fig. 3 STEM images of K1 (a) and K2 (b) photocatalysts.

Interestingly, two distinct dye degradation rate constants are observed in the presence of the K1 photocatalyst, Fig. 4. At longer times, the rate constants tend to increase, mainly for k_{miner}, which can be related to the increase in the concentration of reactive oxygen species (ROS) produced by the excited photocatalyst as the reaction takes place, since the concentration of the organic species is continuously decreasing.[62]

The results are suggestive of the positive effect of doping with nitrogen on the photocatalytic activity. Neither the discoloration nor the mineralization efficiencies achieved using the bare TiO_2 reach the values obtained using K1. The best results for discoloration and mineralization achieved by the bare TiO_2 correspond, respectively, to 76% and 45% of the results reached using K1. On the other hand, the mineralization achieved by the catalyst K2 corresponds to about 12% of that reached using K1.

The K1 photocatalyst was also more effective under solar irradiation than the non-doped TiO_2. 15 mg L^{-1} of the P4R dye solutions were exposed to solar radiation in the presence of 100 mg L^{-1} of K1 and the bare TiO_2 photocatalysts. The discoloration and mineralization efficiencies were measured

Table 4 Conditions for the preparation of catalysts K1 and K2, defined by experimental planning

	Processing conditions		
Variable	K1	K2	TiO_2
Water temperature (1)	3 °C	3 °C	3 °C
Stirring (2)	Magnetic	Ultrasound	Magnetic
Doping (3)	NH_4OH	Urea	—
Reaction time (4)	2 h	2 h	2 h
Sintering temperature (5)	333 °C	500 °C	333 °C
Sintering time	4.2 h	3.0 h	4.2 h
Specific surface area ($m^2\ g^{-1}$)	63.03	12.82	98.86
Total pore volume ($cm^3\ g^{-1}$)	0.14	0.08	0.24
Average pore size (nm)	6.45	19.4	8.11
Discoloration (%)	100	68	76
k_{disc} (min^{-1})	2.2×10^{-2} 5.8×10^{-2}	7.6×10^{-3}	1.0×10^{-2}
Mineralization (%)	64	8	29
k_{miner} (min^{-1})	4.5×10^{-3} 1.0×10^{-2}	$\sim 10^{-4}$ [a]	2.3×10^{-3}

[a] It was not possible to accurately determine k_{miner} for K2 due to the low mineralization observed and the high dispersion of the experimental values.

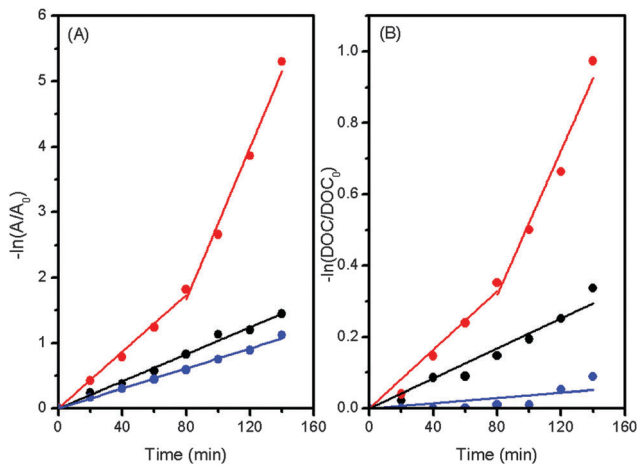

Fig. 4 Kinetics of discoloration (A) and mineralization (B) of a P4R solution in the presence of 100 mg L^{-1} of bare TiO_2 (●), K1 (●) and K2 (●).

as a function of the cumulative UV-A dose. After a 200 kJ m^{-2} UV-A dose in the presence of K1, the total discoloration of the dye solution was observed, while complete mineralization of the organic matter is observed after 600 kJ m^{-2}. Using the bare TiO_2, complete discoloration is observed only after 600 kJ m^{-2} of UV-A radiation, corresponding to 78% mineralization efficiency.

X-ray diffraction patterns of the three catalysts are presented in Fig. 5. For all samples the diffraction peaks can be indexed according to the anatase polymorph (JCPDS 89-4921). A small peak at 30 °C observed for the bare TiO_2 can be associated with the brookite metastable TiO_2 phase (JCPDS 89-4921). Rietveld analyses of the XRD data (Fig. S4 and Table S3, ESI†) allow estimating the amount of brookite as *ca.* 17%. In relation to the bare TiO_2, the lattice parameters of K1 do not vary significantly. Just a small reduction in the anatase cell volume is observed. In relation to K2, the K1 photocatalyst exhibits broader diffraction peaks, which is indicative of poorer crystallinity and smaller particle size. This behavior was expected since the sintering temperature of K1 was lower than that applied for K2. The crystallite size estimated by the Scherrer equation was 14, 23 and 8 nm, respectively, for K1, K2, and bare TiO_2.

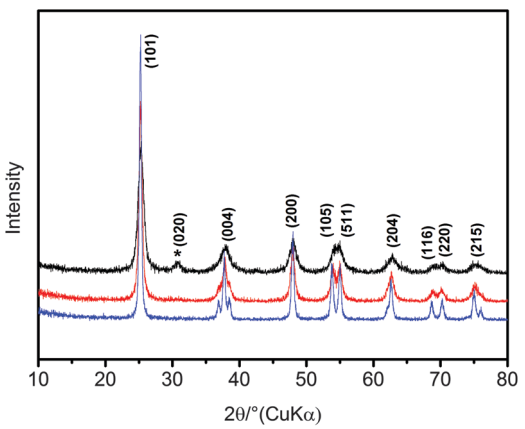

Fig. 5 X-ray diffraction patterns of TiO_2 (—), K1 (——) and K2 (——). * indicates the presence of brookite in the bare TiO_2.

Raman spectroscopy was employed to evaluate the structural disorder of the different oxides prepared, Fig. 6. At first view, it is observed that all investigated samples present the well-known Raman bands for anatase TiO_2 nanoparticles.[63] The more intense E_g mode is located at 144 cm^{-1}, and the other three B_{1g}, A_{1g} and E_g modes are located at 398, 517 and 640 cm^{-1}, respectively. A small peak is also observed at around 200 cm^{-1} and it is assigned to the other E_g frequency mode.

It is noticeable, from the inset of Fig. 6(a), that K1 exhibits a significant reduction of the width for the more intense band in relation to the bare oxide prepared under the same conditions. Such a narrowing is not expected for a doped sample, in which a higher disorder degree is presumed. However, it is clear from XRD data that the bare oxide contains ~17% of brookite content. Brookite TiO_2 exhibits an intense Raman peak at 152 cm^{-1},[64] which can be deconvoluted to the anatase peak at 144 cm^{-1} for the bare TiO_2 sample by using Lorentzian curves, Fig. 6(b). Thus, it is not possible to obtain further information about the influence of nitrogen on the oxide structure from the Raman data since the peak widths of the samples are influenced by the presence of a second phase in the bare oxide. Nevertheless, the absence of large shifts between the samples indicates that the nitrogen probably is being adsorbed at the surface of the TiO_2 structure.

XPS spectroscopy was employed to provide experimental evidence of the chemical states of nitrogen in the samples. XPS data of the K1 photocatalyst reveal the presence of only titanium, oxygen and nitrogen in the surface along with traces of carbon (as typically observed for samples that had contact with air). The high resolution XPS spectra of the K1 photocatalyst before and after the sintering step in the respective N1s, Ti2p and O1s peak regions are shown in Fig. 7.

Before the sintering step at 330 °C, one can observe a broad peak at the N1s region, which can be deconvoluted into two peaks centered at 398.2 and 401.2 eV. Previous XPS studies on N-doped TiO_2 have identified different chemical states for the nitrogen species on TiO_2. N1s peaks with binding energies between 396 and 397 eV are correlated with substitutional nitrogen on oxygen sites, *i.e.* nitride species (Ti–N).[19,31,65]

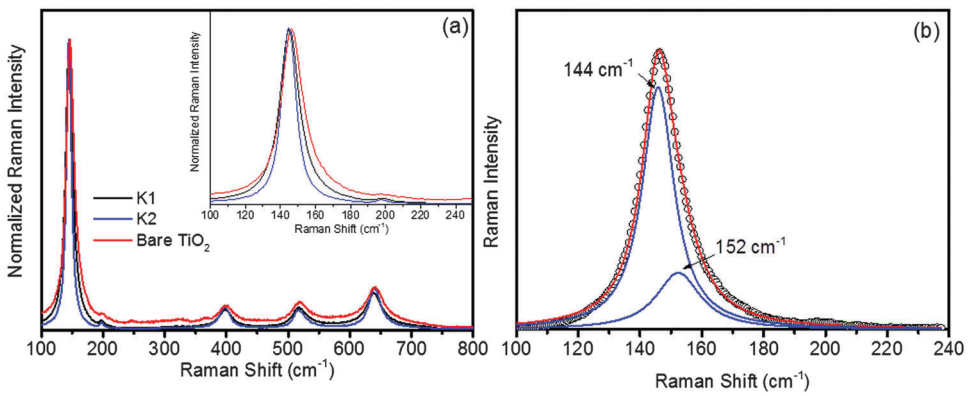

Fig. 6 (a) Raman spectra, at room temperature, for K1 (black line), K2 (blue line) and bare TiO_2 (red line) and (b) theoretical fitting (red line), employing Lorentzian curves (blue lines), of experimental data obtained for the bare TiO_2 (open circles). The inset of (a) shows a zoom of the spectral region between 100 and 240 cm^{-1}.

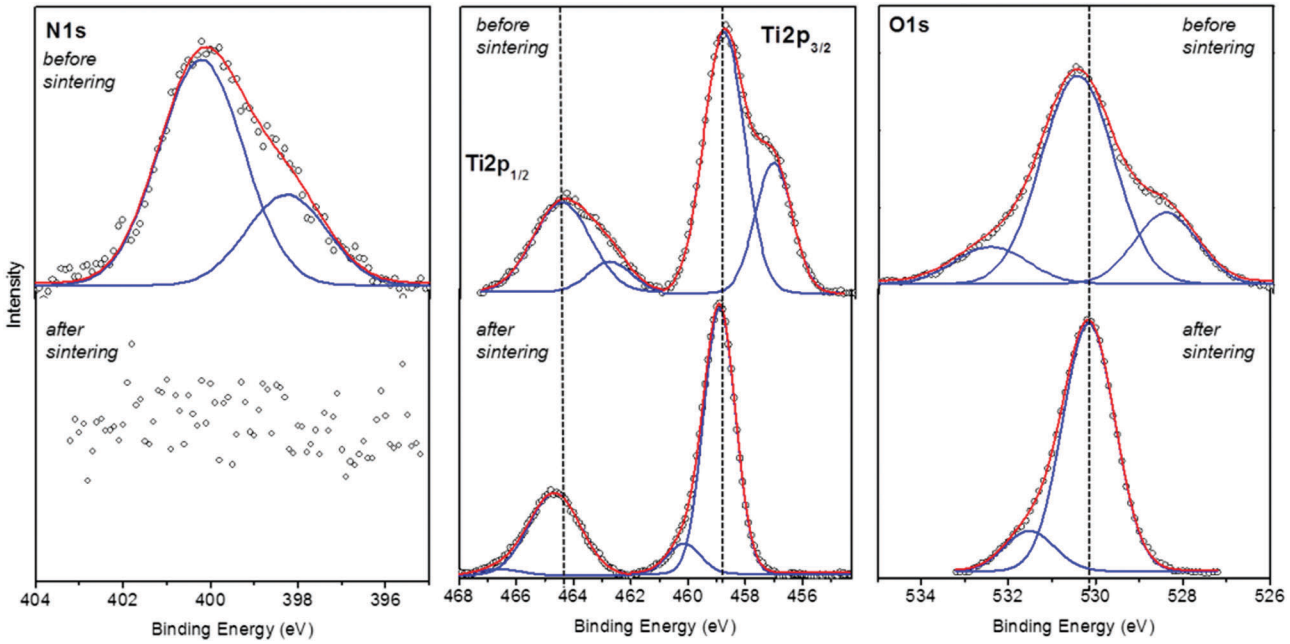

Fig. 7 XPS spectra of the K1 photocatalyst before and after sintering in air at 330 °C. The experimental data (open circles) were deconvoluted using Gaussian functions (solid lines).

On the other hand, peaks in the range of 398–401 eV are related to NO_x and NH_x species adsorbed on the TiO_2 surface.[52,66] Based on the preparation method employed for K1, the N1s peaks observed before sintering can be associated mainly with NH_x species adsorbed on the oxide surface. Additional experimental evidence for this conclusion is taken from FTIR spectra (Fig. S5, ESI†), whereas typical N–H stretching modes at 3186 and 1396 cm^{-1} are observed.[67,68] The N1s XPS peak at higher energies (401.2 eV) can be attributed to NH_4^+ cations adsorbed to $Ti–O^-$ sites (Ti–O–N bonds). This attribution is corroborated by the high resolution spectrum in the O1s region, Fig. 7. The peak at 532.5 eV is shifted in relation to typical Ti–OH signals at 531.5 eV (seen in the spectrum of the sintered sample) and is related to Ti–O–N bonds.[69,70] The main peak at 530.4 eV is due to lattice oxygen (Ti–O–Ti) in the anatase nanocrystals.[71]

The second N1s peak at 398.2 eV can possibly be related to NH_3 molecules coordinated to Ti^{4+} ions in the surface of the oxide to yield O–Ti–N bonds. The K1 photocatalyst is prepared at pH = 8, in which *ca.* 10% of NH_3 remains non-ionized. Thus, they can act as Lewis bases and coordinate to the Ti^{4+} ions in the oxide surface. The high resolution XPS spectrum in Ti2p confirms such assignment. One can observe two components in each peak of the Ti2p doublet. Taking $Ti2p_{3/2}$, a main peak can be seen at 458.8 eV, characteristic of Ti^{4+} ions in anatase,[19,31,65] with a shoulder at 457.1 eV, which is related to electron-richer titanium centers (Ti^{3+}). During the preparation of K1, it is not reasonable to expect the reduction of Ti^{4+} ions, and so, this lower energy $2p_{3/2}$ peak is likely related to Ti^{4+} ions coordinated to NH_3, which acts as a sigma donor. This change in the electronic environment of some Ti^{4+} ions should also be responsible for a third well-resolved O1s peak at 528.4 eV.

After the thermal treatment at 330 °C in air, N1s signals could not be detected, showing that most of the adsorbed species are removed, probably as gaseous NO or NO_2. Thus, from XPS, it can be concluded that less than 2% of the oxide surface is composed of nitrogen species. This low incorporation of nitrogen in the sample agrees with the literature in which the reported nitrogen content in the N-doped TiO_2 varies vastly from 0.08 to 8%. Low concentrations of nitrogen have been generally observed to be all interstitial, which is the case in K1.[72] Concomitantly to the disappearance of the N1s signal, the additional peaks initially observed in the Ti2p and O1s regions also vanish, confirming the previous assignments. In the Ti2p doublet region, a small contribution ($\sim$10%) of a higher energy component is identified and can possibly be related to non-stoichiometric TiO_x species ($x < 2$).

Although XPS data show that most nitrogen species are removed after sintering, different techniques provide clear evidence about its effect on the electronic properties of a TiO_2 matrix. In the diffuse reflectance spectra of K1, K2 and bare TiO_2, Fig. 8, one can observe that K1 exhibits an additional absorption band in the 390–500 nm region. In fact, K1 is a yellow powder, different from the typical white TiO_2 (Fig. 8, inset). This new absorption feature leads to an improvement in the light-harvesting efficiency and, consequently, in the production of reactive oxygen species, responsible for dye degradation. The K1 spectrum resembles the one calculated for $TiO_{2-x}N_x$ by Asahi and co-workers.[73] The new absorption feature in the visible region is attributed to the creation of intermediate electronic levels between the valence and conduction bands of TiO_2 as a result of the interaction between the 2p states of nitrogen and oxygen and also due to the creation of oxygen vacancies during the sintering step that is favored in the presence of nitrogen species.[72–77]

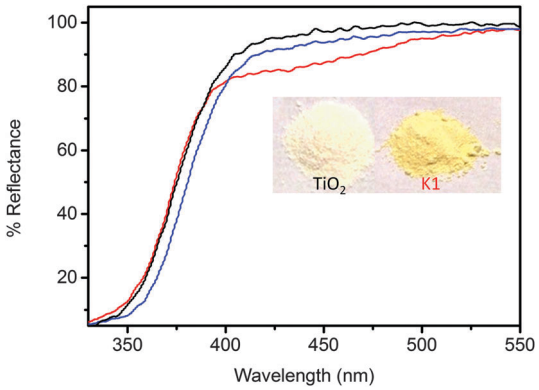

Fig. 8 Diffuse reflectance spectra of the photocatalysts TiO_2 (—), K1 (——) and K2 (——). Inset: Appearance of the powders of the bare TiO_2 and K1.

The presence of intra-band gap states in the form of oxygen vacancies below the conduction band or N 2p localized states slightly above the valence band edge changes the electron–hole dynamics in K1 in relation to the bare TiO_2, as can be inferred from ns-transient absorption measurements. In Fig. 9(a–c), the transient absorption spectra of both photocatalysts at different time-delays as well as data for K2 are shown. The samples exhibit similar transient absorption features with a band at 380–500 nm and a broad band between 500 and 700 nm. In a previous work, we have intensively discussed the origin of these features[55] as a sum of transient absorption signatures that originated from trapped holes and electrons. The trapped electron absorption occurs between 400 and 650 nm, while below 400 nm the transient absorption spectra seem to be dominated by the trapped holes.

The transient absorption intensities between 450 and 600 nm for the bare oxide and for K2 are higher than those observed for K1, especially, which is indicative of multiple trapping sites. For the K1 photocatalyst, it seems that preferential trapping sites are populated upon excitation, leading to narrower bands. Looking at the decay traces at 400 nm, Fig. 9(d), one can observe that K1 exhibits slower recombination rates than the bare oxide and K2. The calculated half-lives are 490, 530 and 870 ns, respectively, for the bare TiO_2, K2 and K1. Thus, the electron–hole lifetime in K1 is almost twice that in K2 and the bare TiO_2.

Therefore, the higher efficiency of K1 as a photocatalyst seems to be originated from its greater light harvesting and slower recombination rates, which are both related to the modification of the TiO_2 matrix caused by nitrogen species. Despite most of them being removed during the sintering processes, they induce the formation of oxygen vacancies at the oxide surface that reduce the band gap energy and, upon excitation, work as electron traps.

4. Conclusions

Factorial experimental planning was successfully employed to obtain N-doped TiO_2 photocatalysts by the precipitation

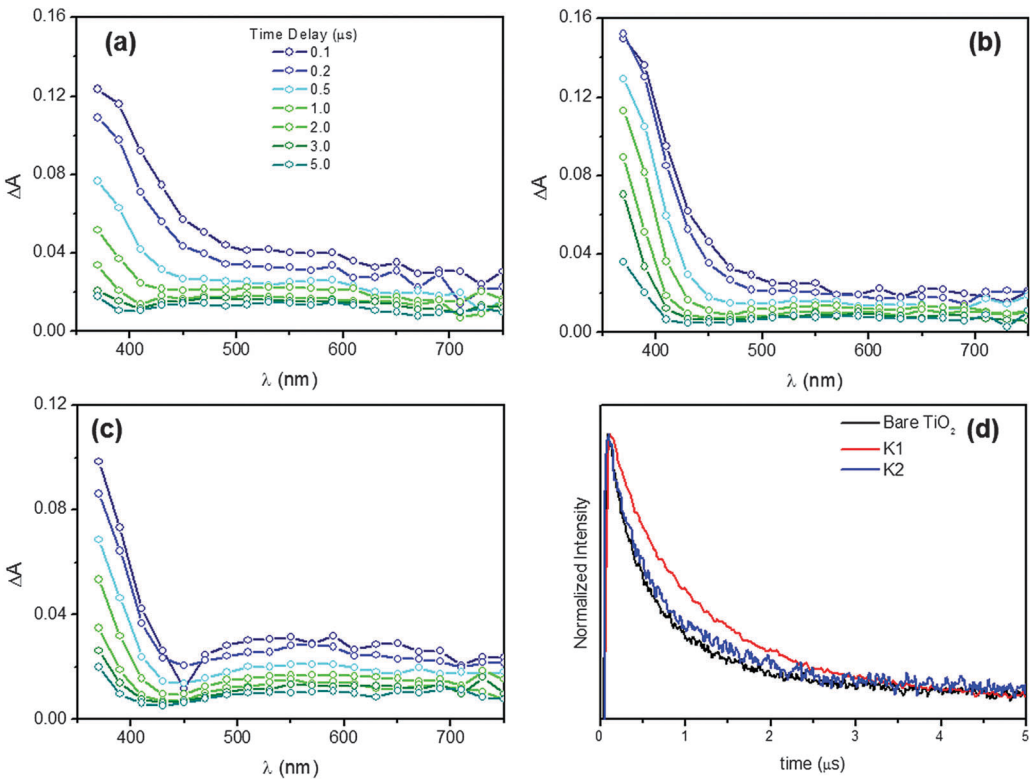

Fig. 9 Transient absorption spectra measured for bare TiO_2 (a), K1 (b) and K2 (c) under air at different time scales following the laser pulse (351 nm; 14 mJ). In (d) is shown the decay traces probed at 400 nm.

method with enhanced activity under solar radiation. The homogeneity of the reaction medium as well as the nitrogen source employed are key variables to obtain samples with suitable morphological properties for photocatalysis. Further thermal treatment is also necessary to ensure the crystallinity of the material and an optimized range of 330–400 °C for 3–5 hours was identified based on the photocatalytic test made using Pounceau 4R dye solutions. Photodegradation tests performed under UV-A irradiation showed that the best N-TiO_2 photocatalyst (K1) can mineralize the P4R dye with rate constants up to 10^{-2} min^{-1}. This catalyst also exhibited a 28% improvement in relation to the non-doped oxide under solar irradiation. Surface characterization techniques show that the nitrogen content in the best photocatalyst is below 2%. Nevertheless, the powder contains oxygen vacancies that introduce intra-gap electronic states allowing visible light absorption and result in an electron–hole half-lifetime of 870 ns, as measured by transient absorption studies. This value is two times higher than the half-lifetime measured for the non-doped oxide. The results presented here provide new insights into the application of factorial design to obtain efficient systems for photocatalysis and can be used for other oxides and dopants.

Acknowledgements

This work was supported by Fundação de Amparo à Pesquisa do Estado de Minas Gerais (FAPEMIG), Conselho Nacional de Desenvolvimento Científico e Tecnológico (CNPq) and Coordenação de Aperfeiçoamento de Pessoal de Nível Superior (CAPES). The authors are thankful to the Brazilian Nanotechnology National Laboratory for the STEM images and the Grupo de Materiais Inorgânicos do Triângulo (GMIT), a research group supported by FAPEMIG (APQ-00330-14). AOTP is thankful to the DLR Green Talents program for the research stay in Germany. Financial support by the Deutsche Forschungsgemeinschaft (DFG) is gratefully acknowledged (Project Number BA 1137/8-2). NMBN is grateful to graduate Program in Physics from Federal University of Pará due for the use of experimental facilities. AEHM, AOTP and NMBN also are grateful to CNPq for their Research fellowships.

References

1 X. J. Lang, X. D. Chen and J. C. Zhao, *Chem. Soc. Rev.*, 2014, **43**, 473–486.
2 A. E. H. Machado, A. O. T. Patrocinio, M. D. França, L. M. Santos, K. A. Borges and L. F. Paula, in *Materials and processes for energy: communicating current research and technological developments*, ed. A. Méndez-Villas, Formatex, Spain, 2013, pp. 867–879.
3 A. O. T. Patrocinio, L. F. Paula, R. M. Paniago, J. Freitag and D. W. Bahnemann, *ACS Appl. Mater. Interfaces*, 2014, **6**, 16859–16866.
4 I. Vasilyeva, G. Kuzmicheva, A. Pochtar, A. Gainanova, O. Timaeva, A. Dorokhov and V. Podbel'skiy, *New J. Chem.*, 2016, **40**, 151–161.
5 K. K. Akurati, S. S. Bhattacharya, M. Winterer and H. Hahn, *J. Phys. D: Appl. Phys.*, 2006, **39**, 2248–2254.
6 A. Braun, K. K. Akurati, G. Fortunato, F. A. Reifler, A. Ritter, A. S. Harvey, A. Vital and T. Graule, *J. Phys. Chem. C*, 2010, **114**, 516–519.
7 M. F. Atitar, A. A. Ismail, S. A. Al-Sayari, D. Bahnemann, D. Afanasev and A. V. Emeline, *Chem. Eng. J.*, 2015, **264**, 417–424.
8 J. Schneider, M. Matsuoka, M. Takeuchi, J. Zhang, Y. Horiuchi, M. Anpo and D. W. Bahnemann, *Chem. Rev.*, 2014, **114**, 9919–9986.
9 S. M. Gupta and M. Tripathi, *Cent. Eur. J. Chem.*, 2012, **10**, 279–294.
10 S. Izadyar, S. Fatemi and T. Mousavand, *Mater. Res. Bull.*, 2013, **48**, 3196–3203.
11 M. Liu, L. Y. Piao, L. Zhao, S. T. Ju, Z. J. Yan, T. He, C. L. Zhou and W. J. Wang, *Chem. Commun.*, 2010, **46**, 1664–1666.
12 A. E. H. Machado, L. M. Santos, K. A. Borges, P. S. Batista, V. A. B. Paiva, P. S. Müller Jr., D. F. M. Oliveira and M. D. França, in *Solar Radiation*, ed. E. B. Babatunde, INTECH, Rijeka, 2012, vol. 19, pp. 339–378.
13 S. G. Kumar and L. G. Devi, *J. Phys. Chem. A*, 2011, **115**, 13211–13241.
14 C. T. Cherian, M. V. Reddy, T. Magdaleno, C. H. Sow, K. V. Ramanujachary, G. V. S. Rao and B. V. R. Chowdari, *CrystEngComm*, 2012, **14**, 978–986.
15 L. G. Devi and R. Kavitha, *Appl. Catal., B*, 2013, **140**, 559–587.
16 I. El Saliby, L. Erdei, H. K. Shon and J. H. Kim, *J. Ind. Eng. Chem.*, 2011, **17**, 358–363.
17 X. Li, H. Lin, X. Chen, H. Niu, T. Zhang, J. Liu and F. Qu, *New J. Chem.*, 2015, **39**, 7863–7872.
18 V. J. Babu, M. K. Kumar, A. S. Nair, T. L. Kheng, S. I. Allakhverdiev and S. Ramakrishna, *Int. J. Hydrogen Energy*, 2012, **37**, 8897–8904.
19 V. Iliev, D. Tomova and S. Rakovsky, *Desalination*, 2010, **260**, 101–106.
20 S. A. Ansari, M. M. Khan, M. O. Ansari and M. H. Cho, *New J. Chem.*, 2016, **40**, 3000–3009.
21 N. Sharotri and D. Sud, *New J. Chem.*, 2015, **39**, 2217–2223.
22 Z. Zhao and Q. Liu, *J. Phys. D: Appl. Phys.*, 2008, **41**, 025105.
23 J. Graciani, L. J. Alvarez, J. A. Rodriguez and J. F. Sanz, *J. Phys. Chem. C*, 2008, **112**, 2624–2631.
24 M. Sahoo, A. K. Yadav, S. N. Jha, D. Bhattacharyya, T. Mathews, N. K. Sahoo, S. Dash and A. K. Tyagi, *J. Phys. Chem. C*, 2015, **119**, 17640–17647.
25 W. Kim, T. Tachikawa, H. Kim, N. Lakshminarasimhan, P. Murugan, H. Park, T. Majima and W. Choi, *Appl. Catal., B*, 2014, **147**, 642–650.
26 L. Lo Presti, M. Ceotto, F. Spadavecchia, G. Cappelletti, D. Meroni, R. G. Acres and S. Ardizzone, *J. Phys. Chem. C*, 2014, **118**, 4797–4807.
27 W. Qian, P. A. Greaney, S. Fowler, S.-K. Chiu, A. M. Goforth and J. Jiao, *ACS Sustainable Chem. Eng.*, 2014, **2**, 1802–1810.
28 R. P. Vitiello, J. M. Macak, A. Ghicov, H. Tsuchiya, L. F. P. Dick and P. Schmuki, *Electrochem. Commun.*, 2006, **8**, 544–548.
29 C. X. Feng, Y. Wang, Z. S. Jin, J. W. Zhang, S. L. Zhang, Z. S. Wu and Z. J. Zhang, *New J. Chem.*, 2008, **32**, 1038–1047.

30 H. Irie, Y. Watanabe and K. Hashimoto, *J. Phys. Chem. B*, 2003, **107**, 5483–5486.
31 Y. Huang, Z. Xuxu, Y. Zhongyi, T. Feng, F. Beibei and H. Keshan, *Chin. J. Chem. Eng.*, 2007, **15**, 802–807.
32 L. Gomathi Devi and R. Kavitha, *RSC Adv.*, 2014, **4**, 28265–28299.
33 R. Asahi, T. Morikawa, H. Irie and T. Ohwaki, *Chem. Rev.*, 2014, **114**, 9824–9852.
34 W. Zhang, B. P. Jia, Q. Z. Wang and D. Dionysiou, *J. Nanopart. Res.*, 2015, **17**, 221.
35 J. Lynch, C. Giannini, J. K. Cooper, A. Loiudice, I. D. Sharp and R. Buonsanti, *J. Phys. Chem. C*, 2015, **119**, 7443–7452.
36 M. Safaei, R. Sarraf-Mamoory, M. Rashidzadeh and M. Manteghian, *Phys. Status Solidi C*, 2010, **7**, 2727–2730.
37 A. Danion, C. Bordes, J. Disdier, J. Y. Gauvrit, C. Guillard, P. Lanteri and N. Jaffrezic-Renault, *J. Photochem. Photobiol., A*, 2004, **168**, 161–167.
38 C. M. Wang, H. Wu and S. L. Chung, *J. Porous Mater.*, 2006, **13**, 307–314.
39 N. Kumar, A. Bansal, G. S. Sarma and R. K. Rawal, *Talanta*, 2014, **123**, 186–199.
40 L. V. Candioti, M. M. De Zan, M. S. Camara and H. C. Goicoechea, *Talanta*, 2014, **124**, 123–138.
41 M. P. Callao, *Trends Anal. Chem.*, 2014, **62**, 86–92.
42 D. Lutic and I. Cretescu, *Rev. Chim.*, 2016, **67**, 134–138.
43 H. Khalilian, A. Semnani, A. Rinnan and H. Haddadi, *Anal. Methods*, 2016, **8**, 4293–4299.
44 S. M. Liu, S. Kokot and G. Will, *J. Photochem. Photobiol., C*, 2009, **10**, 159–172.
45 C. Miranda, J. Yanez, D. Contreras, R. Garcia, W. F. Jardim and H. D. Mansilla, *Appl. Catal., B*, 2009, **90**, 115–119.
46 P. Palacios, C. Lizama, C. Caneo and M. Ollino, *J. Adv. Oxid. Technol.*, 2007, **10**, 67–71.
47 B. Baeza, C. Lizama, C. Caneo and M. Ollino, *J. Adv. Oxid. Technol.*, 2007, **10**, 411–414.
48 D. L. Marchisio, F. Omegna, A. A. Barresi and P. Bowen, *Ind. Eng. Chem. Res.*, 2008, **47**, 7202–7210.
49 X. X. Fu, B. B. Wang, C. Chen, Z. M. Ren, C. Y. Fan and Z. Y. Wang, *New J. Chem.*, 2014, **38**, 4754–4759.
50 E. Luevano-Hipolito, A. Martinez-de la Cruz, E. Lopez-Cuellar, Q. L. Yu and H. J. H. Brouwers, *Mater. Chem. Phys.*, 2014, **148**, 208–213.
51 E. P. Barrett, L. G. Joyner and P. P. Halenda, *J. Am. Chem. Soc.*, 1951, **73**, 373–380.
52 Y. Wang, C. X. Feng, M. Zhang, J. J. Yang and Z. J. Zhang, *Appl. Catal., B*, 2010, **100**, 84–90.
53 L. M. Santos, W. A. Machado, M. D. Franca, K. A. Borges, R. M. Paniago, A. O. T. Patrocinio and A. E. H. Machado, *RSC Adv.*, 2015, **5**, 103752.
54 A. O. T. Patrocínio, E. B. Paniago, R. M. Paniago and N. Y. Murakami Iha, *Appl. Surf. Sci.*, 2008, **254**, 1874–1879.
55 A. O. T. Patrocinio, J. Schneider, M. D. Franca, L. M. Santos, B. P. Caixeta, A. E. H. Machado and D. W. Bahnemann, *RSC Adv.*, 2015, **5**, 70536–70545.
56 T.-P. Lin and H. K. A. Kan, *J. Opt. Soc. Am.*, 1970, **60**, 1252–1256.
57 R. W. Kessler, G. Krabichler, S. Uhl, D. Oelkrug, W. P. Hagan, J. Hyslop and F. Wilkinson, *Optica Acta*, 1983, **30**, 1099–1111.
58 D. F. M. Oliveira, P. S. Batista, P. S. Muller, Jr., V. Velani, M. D. Franca, D. R. de Souza and A. E. H. Machado, *Dyes Pigm.*, 2012, **92**, 563–572.
59 A. Di Paola, E. Garcia-Lopez, G. Marci and L. Palmisano, *J. Hazard. Mater.*, 2012, **211**, 3–29.
60 L. B. McCusker, F. Liebau and G. Engelhardt, *Microporous Mesoporous Mater.*, 2003, **58**, 3–13.
61 W. Li, Z. X. Wu, J. X. Wang, A. A. Elzatahry and D. Y. Zhao, *Chem. Mater.*, 2014, **26**, 287–298.
62 X. H. Yang, H. T. Fu, A. B. Yu and X. C. Jiang, *J. Colloid Interface Sci.*, 2012, **387**, 74–83.
63 U. Balachandran and N. G. Eror, *J. Solid State Chem.*, 1982, **42**, 276–282.
64 M. N. Iliev, V. G. Hadjiev and A. P. Litvinchuk, *Vib. Spectrosc.*, 2013, **64**, 148–152.
65 Y. Cong, J. L. Zhang, F. Chen and M. Anpo, *J. Phys. Chem. C*, 2007, **111**, 6976–6982.
66 J. J. Qian, G. J. Cui, M. J. Jing, Y. Wang, M. Zhang and J. J. Yang, *Int. J. Photoenergy*, 2012, 198497.
67 C. Y. Yan, K. F. Chen, C. H. Lai, S. W. Lai, Q. Chang and Y. P. Peng, *J. Environ. Sci.*, 2014, **26**, 1505–1512.
68 M. Zalas, *Catal. Today*, 2014, **230**, 91–96.
69 G. A. Battiston, R. Gerbasi, A. Gregori, M. Porchia, S. Cattarin and G. A. Rizzi, *Thin Solid Films*, 2000, **371**, 126–131.
70 Y. Cong, J. Zhang, F. Chen and M. Anpo, *J. Phys. Chem. C*, 2007, **111**, 6976–6982.
71 U. Diebold, *Surf. Sci. Rep.*, 2003, **48**, 53–229.
72 C. Di Valentin, G. Pacchioni, A. Selloni, S. Livraghi and E. Giamello, *J. Phys. Chem. B*, 2005, **109**, 11414–11419.
73 R. Asahi, T. Morikawa, T. Ohwaki, K. Aoki and Y. Taga, *Science*, 2001, **293**, 269–271.
74 C. Di Valentin, G. Pacchioni and A. Selloni, *Phys. Rev. B: Condens. Matter Mater. Phys.*, 2004, **70**, 085116.
75 J. Y. Lee, J. Park and J. H. Cho, *Appl. Phys. Lett.*, 2005, **87**, 011904.
76 H. Wang and J. P. Lewis, *J. Phys.: Condens. Matter*, 2006, **18**, 421–434.
77 K. S. Yang, Y. Dai, B. B. Huang and S. H. Han, *J. Phys. Chem. B*, 2006, **110**, 24011–24014.